IOP Publishing | Institute of Physics and Engineering in Medicine Physics in Medicine and Biology

Phys. Med. Biol. **59** (2014) 1165–1187 doi:10.1088/0031-9155/59/5/1165

Evaluation of radiation dose to anthropomorphic paediatric models from positron-emitting labelled tracers

Tianwu Xie[1] **and Habib Zaidi**[1,2,3]

[1] Division of Nuclear Medicine and Molecular Imaging, Geneva University Hospital, CH-1211 Geneva 4, Switzerland
[2] Geneva Neuroscience Center, Geneva University, CH-1205 Geneva, Switzerland
[3] Department of Nuclear Medicine and Molecular Imaging, University of Groningen, University Medical Center Groningen, 9700 RB Groningen, Netherlands

E-mail: habib.zaidi@hcuge.ch

Received 28 August 2013, revised 22 January 2014
Accepted for publication 28 January 2014
Published 20 February 2014

Abstract

PET uses specific molecules labelled with positron-emitting radionuclides to provide valuable biochemical and physiological information. However, the administration of radiotracers to patients exposes them to low-dose ionizing radiation, which is a concern in the paediatric population since children are at a higher cancer risk from radiation exposure than adults. Therefore, radiation dosimety calculations for commonly used positron-emitting radiotracers in the paediatric population are highly desired. We evaluate the absorbed dose and effective dose for 19 positron-emitting labelled radiotracers in anthropomorphic paediatric models including the newborn, 1-, 5-, 10- and 15-year-old male and female. This is achieved using pre-calculated *S*-values of positron-emitting radionuclides of UF-NCI paediatric phantoms and published biokinetic data for various radiotracers. The influence of the type of anthropomorphic model, tissue weight factors and direct human- versus mouse-derived biokinetic data on the effective dose for paediatric phantoms was also evaluated. In the case of ^{18}F-FDG, dosimetry calculations of reference paediatric patients from various dose regimens were also calculated. Among the considered radiotracers, ^{18}F-FBPA and ^{15}O-water resulted in the highest and lowest effective dose in the paediatric phantoms, respectively. The ICRP 103 updated tissue-weighting factors decrease the effective dose in most cases. Substantial differences of radiation dose were observed between direct human- versus mouse-derived biokinetic data. Moreover, the effect of using voxel- versus MIRD-type models on the calculation of the effective dose was also studied. The generated database of absorbed organ dose and effective dose for various positron-emitting labelled radiotracers using new generation computational models and the new ICRP

tissue-weighting factors can be used for the assessment of radiation risks to paediatric patients in clinical practice. This work also contributes to a better understanding of the factors influencing patient-specific radiation dose calculation.

Keywords: radiation dosimetry, PET, radiotracers, Monte Carlo, paediatrics

S Online supplementary data available from stacks.iop.org/PMB/59/1165/mmedia

(Some figures may appear in colour only in the online journal)

1. Introduction

The noninvasive nature of positron emission tomography (PET) makes it an extremely useful tool for clinical diagnosis, staging, treatment and surveillance of various diseases (Gambhir 2002). Because of its high sensitivity and target specificity for the paediatric population, PET enables the detection and characterization of disease in its earliest stages and provides valuable diagnostic information that may not be easily obtained using conventional imaging techniques (Tatsumi *et al* 2007, Treves *et al* 2011, Kleis *et al* 2009). However, the exposure of paediatric patients to ionizing radiation during standalone or hybrid medical imaging examinations is a matter of concern (Chawla *et al* 2010, Fahey *et al* 2011). In this regard, some improved dose regimens and dedicated paediatric PET/CT protocols have been devised and published by various investigators (Accorsi *et al* 2010, Jacobs *et al* 2005, Gelfand 2010, Alessio *et al* 2009) and professional societies (Gelfand *et al* 2011, Lassmann *et al* 2007).

With the same absolute level of radiation dose, children may experience greater stochastic effects from ionizing radiation than adults because they have a proportionally higher percentage of replicating cells, which are more radiosensitive than other cells (Robbins 2008). The stochastic effects (e.g. cancer and hereditary effects) are mainly caused by radiation-induced DNA mutation or symmetrical translocations in cells (Mothersill and Seymour 2013, Prasad *et al* 2004), and follow a latent period varying from 2 years to 30 years (Steinert *et al* 2003, Parker *et al* 2005). Since children have longer post-irradiation life period for the emergence of deleterious stochastic effects, they are at higher cancer risk from ionizing radiation compared to adults. In this context, the accurate assessment of radiation dose delivered to the paediatric population involving the use of positron-emitting labelled radiotracers for standalone or hybrid diagnostic imaging techniques (e.g. PET, PET-CT) is of paramount importance in clinical practice.

To this end, organ absorbed doses are often estimated using anthropomorphic computational phantoms and Monte Carlo calculations (Zaidi 1999). These phantoms and computer codes respectively mimic the morphology and internal anatomic structures of children and simulate the interaction of ionizing radiation with biological tissues, thus allowing tracking the transport of radiation in the human body. Depending on the geometric features used to define the anatomical model for radiation transport calculations, computational models can be divided into three types (Zaidi and Xu 2007): stylized models which employ simple equation-based mathematical functions, voxel-based models which use matrices obtained from segmented cryosection or medical (CT or MR) images, and hybrid equation-voxel based models which combine the two aforementioned modelling approaches. In most studies reported in the literature (Eberlein *et al* 2011, Chawla *et al* 2010), the estimation of organ absorbed dose from PET radiotracers to the paediatric population were performed using the dosimetric characteristics of positron-emitting tracers and mathematical paediatric phantoms

specified in ICRP publications (ICRP 1988, 1998, 2008), MIRDOSE (Stabin 1996) or OLINDA (Stabin *et al* 2005) packages. However, significant differences were reported between dosimetric results of stylized and voxel-based models of the same subject (Petoussi-Henss *et al* 2007). To estimate the potential detrimental effects of ionizing radiation, the effective dose is calculated by summing the products of organ absorbed dose and the ICRP recommended tissue-weighting factors. The published reports used the ICRP 60 tissue-weighting factors for effective dose calculation in the paediatric population (ICRP 1988, 1998, 2008), although new tissue-weighting factors were published in ICRP Publication 103 (Bolch *et al* 2009). Differences of 21% to 31% have been reported for the estimates of effective dose between the ICRP 60 and ICRP 103 tissue-weighting factors (Boetticher *et al* 2008). Therefore, the assessment of organ absorbed dose and effective dose for commonly used positron-emitting radiotracers in new generation anthropomorphic paediatric phantoms according to the new ICRP tissue-weighting factors is highly desired.

In nuclear medicine, paediatric imaging protocols are usually extrapolated from adult imaging guidelines. The administered radiotracer activity to paediatric patients varies widely on the basis of clinical experience and preference of physicians (Treves *et al* 2008). A number of guidelines and methodologies were developed for the calculation of paediatric PET/CT injected activity in an effort to provide guidance on optimal imaging protocols (Gelfand *et al* 2011, Accorsi *et al* 2010, Lassmann *et al* 2007, Alessio *et al* 2009, Churchill 1964, Gelfand 2010, Du Bois and Du Bois 1916, 1989). Since an optimal imaging protocol would result in images with sufficient diagnostic quality at minimum radiation risk (Alessio *et al* 2011), it is important to evaluate the dosimetric aspect of different dose regimens in paediatric imaging.

The biokinetic data derived from small animals were used to estimate human radiation dose of new radiotracers. Sakata *et al* (2013) reported significant discrepancy between direct human- and mouse-derived organ doses and effective dose for adults. However, the direct comparison of animal- and human-derived radiation dose for the paediatric population has not been reported so far.

In this work, human biodistribution data of 19 positron-emitting labelled radiotracers were obtained from published literature (ICRP 1988, 1998, 2008, Sakata *et al* 2013). Organ absorbed doses and effective dose were calculated using these biokinetic data, Monte Carlo calculated *S*-values of positron-emitting radionuclides of the University of Florida-National Cancer Institute (UF-NCI) family of paediatric models, and the ICRP 103 tissue-weighting factors. The obtained radiation dose database can be used to assess the deterministic and stochastic effects to children undergoing PET imaging procedures at different ages. The dosimetric properties of different dose regimens for ^{18}F-FDG, taken as an example as the most widely used tracer, were also calculated for the paediatric phantoms used in this work. A detailed knowledge of the influence of the type of anthropomorphic model, tissue-weight factor, dose regimen and human/mouse-derived biokinetic data on the effective dose to the paediatric population may advance the understanding of the uncertainties involved in internal radiation dosimetry calculations.

2. Materials and methods

2.1. Radiotracers

The radiotracers investigated in this work are ^{18}F-FDG (Reivich *et al* 1985), ^{11}C-acetate (Visser 2001, Albrecht *et al* 2007), ^{11}C- and ^{18}F-amino acids, ^{11}C-methionine (Huang and McConathy 2013), ^{11}C- and ^{18}F-brain receptor substances (ICRP 2008), ^{11}C-thymidine, [Methyl-^{11}C]-thymidine (Goethals *et al* 1996), ^{11}C-SA4503 (Toyohara *et al* 2009), ^{11}C-MPDX

Table 1. List of abbreviations used in this work.

Acronyms	
GB	Gall bladder
SI	Small intestine
UB	Urinary bladder
OCL	Oral cavity layer
ET region	Extrathoracic region
^{11}C-SA4503	^{11}C-1-(3,4-dimethoxyphenethyl)-4-(3-phenylprophyl)piperazine
^{11}C-MPDX	^{11}C-8-dicyclopropylmethyl-1-methyl-3-propylxanthine
^{11}C-TMSX	^{11}C-(*E*)-8-(3,4,5-trimethoxystyryl)-1,3,7-trimethylxanthine
^{11}C-CHIBA-1001	4–^{11}C-methylphenyl 1,4-diazabicyclo[3.2.2.]nonane-4-carboxylate
^{11}C-4DST	^{11}C-4'-thiothymidine
^{18}F-FDG	2-[^{18}F]Fluoro-2-deoxy-D-glucose
^{18}F-L-dopa	6-[^{18}F]Fluoro-L-dopa
^{18}F-FBPA	4-borono-2-^{18}F-fluoro-L-phenylalanine
^{68}Ga-EDTA	^{68}Ga-ethylenediaminetetraacetic acid
ICRP	International Commission on Radiological Protection
EANM	European Association of Nuclear Medicine
NECRD	Noise-equivalent count rate density
BSA	Body surface area

(Paul *et al* 2011), ^{11}C-TMSX (Mishina *et al* 2011), ^{11}C-CHIBA-1001, ^{11}C-4DST (Toyohara *et al* 2011), ^{15}O-water (Nesterov *et al* 2009), ^{18}F-L-dopa (Oehme *et al* 2011), ^{18}F-FBPA (Yoshimoto *et al* 2013), and ^{68}Ga-EDTA (Maecke and André 2007). Moreover, the realistic maximum model of ^{11}C (ICRP 2008) was studied. The biokinetic data of these radiotracers were obtained from the supplemental materials of ICRP publication 106 (ICRP 2008) and (Sakata *et al* 2013). The list abbreviations (radiotracers, organs, quantities) used in this work are summarized in table 1. The application, source organs containing high activity concentration and the sources of the biodistribution data of the various radiotracers used in this work are listed in table 2.

2.2. Definition of organs and tissues for dose calculation

The UF-NCI hybrid paediatric phantom series, including the reference newborn, 1-, 5-, 10-, and 15-year-old male and female models, were used for radiation dosimetry calculations. Figure 1 shows the front 3D views of the ten paediatric phantoms used in this work. For the sake of convenience in terms of effective dose calculation, homogeneous organs such as the left lung and right lung, the submaxillary salivary gland and sublingual salivary gland, the cartilage, cortical bone and spongiosa at different bone sites were merged as one identified region. The body weights and organ/tissue masses for the paediatric phantoms are summarized in the supplemental table A1 (available from stacks.iop.org/PMB/59/1165/mmedia).

The Monte Carlo N-Particle eXtended code (version 2.5.c) was adopted for radiation transport simulation of positron-emitting sources in the UF-NCI paediatric phantoms. The decay data of the investigated positron-emitting radionuclides were obtained from the Health Physics Society electronic resource (HPS 2013). The energy deposited by photons, electrons, and positrons in organs/tissues were recorded in unit of MeV per particle. An in-house C++ code was developed to calculate the absorbed doses and effective doses in paediatric models for the considered radiotracers using published biokinetic data, currently available

Table 2. List of considered compounds, applications, references of adopted biokinetic data and identified source organs containing high activity concentration.

		References for biokinetic data			
Radiopharmaceutical	Studies	ICRP publication 80	ICRP publication 106	Sakata *et al* (Sakata *et al* 2013)	Source organs[a]
^{11}C-Acetate	Myocardial oxidative metabolism (Visser 2001) and renal, pancreatic and prostate cancer (Albrecht *et al* 2007)		x		Heart wall, liver, pancreas, blood, kidney
^{11}C-Amino acids	Protein synthesis (Huang and McConathy 2013)		x		Brain, liver, lung, pancreas, SI wall, spleen, thyroid, UB content, blood vessel, muscle, ovaries/testes, kidney
^{11}C-Brain receptor substances	Molecular imaging of different brain receptors (ICRP 2008)		x		Brain, colon content, GB content, SI content, UB content
^{11}C-Methionine	Protein synthesis (Huang and McConathy 2013)				Brain, colon content, GB content, liver, lung, pancreas, SI content, spleen, UB content, kidney
[Methyl-^{11}C]-Thymidine	Cell proliferation in malignant tumours (Goethals *et al* 1996)	x	x		Liver, blood, muscle, kidney
^{11}C-Thymidine	Cell proliferation in malignant tumours (Goethals *et al* 1996)	x			Liver, blood, kidney
^{11}C-SA4503	Sigma1 receptor (Toyohara *et al* 2009)			x	Brain, heart wall, liver, lung, pancreas, spleen, thyroid, kidney, SI, stomach, UB
^{11}C-MPDX	Adenosine A1 receptor (Paul *et al* 2011)			x	Brain, heart wall, liver, lung, thyroid, kidney, SI, stomach, UB
^{11}C-TMSX	Adenosine A2A receptor (Mishina *et al* 2011)			x	Brain, heart wall, liver, lung, thyroid, GB, kidney, SI, stomach, UB
^{11}C-CHIBA-1001	DNA synthesis (Toyohara *et al* 2011)			x	Brain, heart wall, liver, lung, pancreas, spleen, thyroid, GB, kidney, SI, stomach, UB

Table 2. (Continued.)

Radiopharmaceutical	Studies	References for biokinetic data: ICRP publication 80	ICRP publication 106	Sakata *et al* (Sakata *et al* 2013)	Source organs[a]
^{11}C-4DST	DNA synthesis (Toyohara *et al* 2011)			x	Heart wall, liver, lung, spleen, spongiosa, kidney, SI, UB
^{15}O-water	Blood flow measurement (Nesterov *et al* 2009)	x			Adrenal, brain, colon wall, heart wall, heart content, liver, lung, pancreas, SI wall, spleen, stomach wall, thyroid, muscle, ovaries/testes, kidney, skeleton
^{18}F-Amino acids	Protein synthesis (Huang and McConathy 2013)		x		Brain, liver, lung, pancreas, SI wall, spleen, thyroid, UB content, blood vessel, muscle, ovaries/testes, kidney
^{18}F-Brain receptor substances	Molecular imaging of different brain receptors (ICRP 2008)		x		Brain, colon content, GB content, liver, lung, SI content, stomach wall, stomach content, thyroid, UB content, kidney
^{18}F-FDG	Glucose metabolism (Reivich *et al* 1985)		x		Brain, heart wall, liver, lung, UB content
^{18}F-L-dopa	Dopamine metabolism and dopaminergic function (Oehme *et al* 2011)		x		Kidney, UB content
^{18}F-FBPA	Effect prediction of boron neutron capture therapy (Yoshimoto *et al* 2013)			x	Brain, heart wall, liver, lung, spleen, thyroid, spongiosa, kidney, stomach, UB
^{68}Ga-EDTA	Renal function investigation (Maecke and André 2007)	x			UB content, kidney
Realistic maximum models					
^{11}C			x		UB content

[a] The remaining activity was considered to be uniformly distributed in other organs and tissues.

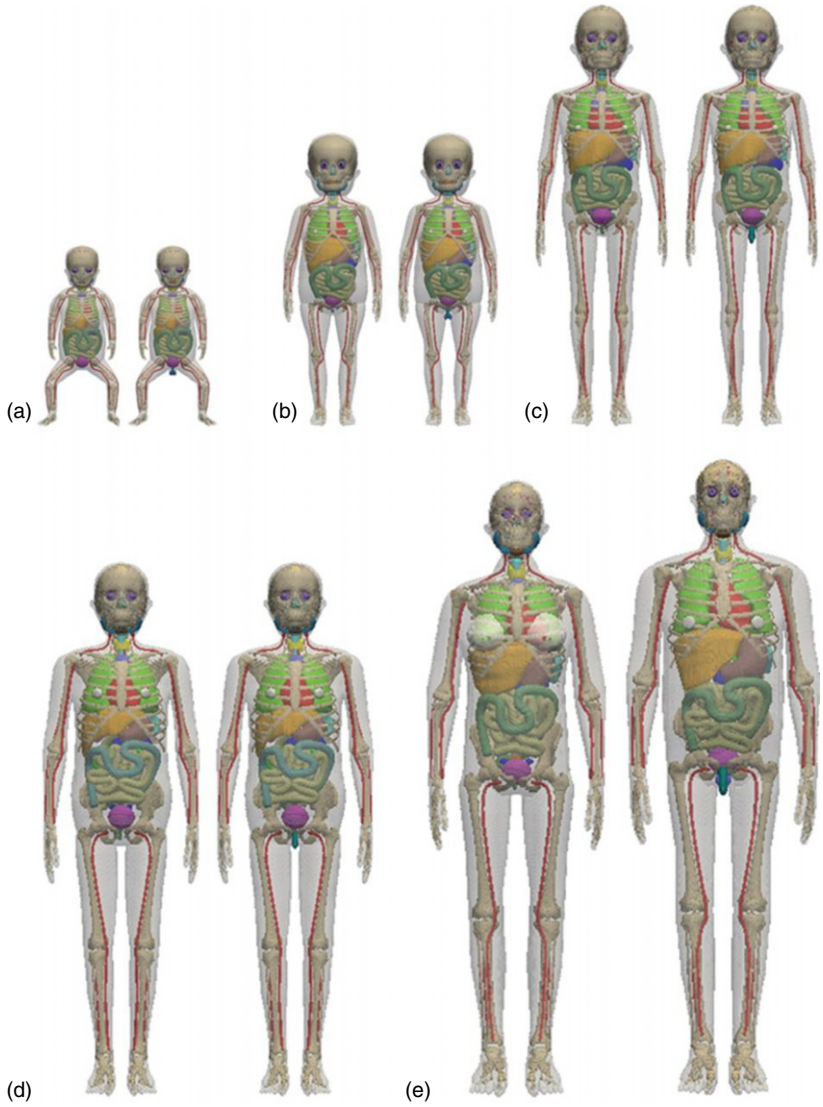

Figure 1. 3D visualization of computational paediatric phantoms showing: (a) the newborn, (b) 1-year, (c) 5-years, (d) 10-years, and (e) 15-years female (left) and male (right) phantoms.

tissue weight factors and the recently evaluated *S*-values of C-11, F-18, O-15 and Ga-68 (Xie *et al* 2013).

The absorbed dose is calculated for 59 target organs/tissues by performing the sum of contributions from radioactive decay occurring in various source organs/tissues. The radiotracer is assumed to be uniformly distributed in the source regions. For source organs without specified biokinetic data, the accumulated activity for radiotracers is determined by multiplying the volume fraction and the accumulated activity quoted for 'other organs and tissues'. The absorbed dose to red bone marrow is approximated by the absorbed dose to

spongiosa for effective dose calculation. The absorbed dose to blood vessels refers to the dose to the blood in the arteries and the veins. The absorbed doses to the colon, gall bladder (GB), heart, small intestine (SI), stomach, urinary bladder (UB), kidney (total) and skeleton (total) refer to the mean absorbed dose for the integrated organ, including the wall and content for colon, GB, heart, SI, stomach, and UB, the cortex, medulla and pelvis for the kidney, and the cortical bone, spongiosa and cartilage for the skeleton. Age-dependent organ mass, biokinetic data and *S*-values were used for the absorbed dose calculation. For all organs except the UB content, the biokinetic data and accumulated activity of radiotracers are similar for adults and children of different ages. For UB content, the accumulated activity of ^{11}C- and ^{18}F-brain receptor substances, ^{18}F-L-DOPA, ^{18}F-FDG, ^{18}F-amino acids and ^{68}Ga-EDTA vary according to the considered paediatric population model. Since the newborn is traditionally considered to empty its bladder automatically (Sillen 2001), the activity concentration of these radiotracers in the UB content is assumed to be identical to 'other organs and tissues'.

2.3. Absorbed dose and effective dose calculations

In radiation biology, clinical radiology, and radiological protection the absorbed dose is the basic physical dose quantity defined as the mean energy imparted to target tissue per unit tissue mass. In the Medical Internal Radiation Dose (MIRD) formalism (Bolch *et al* 2009), the radiation absorbed dose $D\,(r_T, T_D)$ delivered to any target tissue r_T from source organ r_S, over a considered dose-integration period T_D is calculated according to equation (A.1) (see the appendix). The *S*-value describes the equivalent dose rate in the target organ per unit activity in the source organ and depends on the decay scheme of the radionuclide, the type, energy and yield of emitted radiation per nuclear transformation, the mass of the target organ, and the pre-constructed age- and sex-specific anatomical model. In this work, the *S*-values of the considered reference paediatric phantoms for C-11, O-15, F-18 and Ga-68 (Xie *et al* 2013) were employed for absorbed dose calculations.

The detriment caused by radiation to the human body depends on the linear energy transfer of the different types of radiation emitted by the radionuclide. To relate the absorbed dose to stochastic effects, the absorbed dose in organs/tissues is multiplied by the radiation weighting factor and the result is termed the equivalent dose, $H\,(r_T, T_D)$ (equation (A.2)).

To reflect the combined detriment from stochastic effects of equivalent doses in all organs/tissues of the human body, the concept of effective dose was introduced by ICRP (1991, 2007), and is calculated by the sum of the product of tissue-weighting factor (ω_T) and equivalent doses (equation (A.3)). The values of ω_T describe the relative contribution of individual organs/tissues to the overall radiation detriment, thus $\sum_T \omega_T = 1$. The tissue-weighting factors for organs/tissues given by the ICRP Publication 60 (ICRP 1991) and ICRP Publication 103 (ICRP 2007) are summarized in table 3. It should be noted that the ω_T values represent mean values for humans averaged over both sexes and all ages.

If $A(r_S, t)$ is normalized to a unit administered activity A_0, then the absorbed dose to the target tissue and the effective dose in the human body per unit administered activity can be obtained from equations (A.4) and (A.5), respectively.

For the purpose of radiological protection, the ICRP (ICRP 2007) suggests to apply a single value of effective dose for both sexes. The sex-specific equivalent doses are then averaged resulting in equivalent doses of a reference person. The sex-averaged equivalent doses of the reference person are then weighted by the tissue-weighting factors and summed over all organs and tissues for the assessment of the effective dose according to equation (A.6).

Table 3. Recommended tissue-weighting factors of ICRP publication 60 (ICRP 1991) and ICRP publication 103 (ICRP 2007).

	ICRP 60		ICRP 103	
Tissue	Female	Male	Female	Male
Adrenal	–	–	0.01	0.01
Brain	–	–	0.01	0.01
Colon wall	0.12	0.12	0.12	0.12
GB wall	–	–	0.01	0.01
Heart wall	–	–	0.01	0.01
Liver	0.05	0.05	0.04	0.04
Lung	0.12	0.12	0.12	0.12
Pancreas	–	–	0.01	0.01
Salivary glands	–	–	0.01	0.01
SI wall	–	–	0.01	0.01
Spleen	–	–	0.01	0.01
Stomach wall	0.12	0.12	0.12	0.12
Thymus	–	–	0.01	0.01
Thyroid	0.05	0.05	0.04	0.04
UB wall	0.05	0.05	0.04	0.04
Muscle	–	–	0.01	0.01
Cortical bone	0.01	0.01	0.01	0.01
Spongiosa	0.12	0.12	0.12	0.12
Ovaries (♀)	0.2	–	0.08	–
Testes (♂)	–	0.2	–	0.08
Uterus (♀)	–	–	0.01	–
Prostate (♂)	–	–	–	0.01
Breast	0.05	0.05	0.12	0.12
Oesophagus	0.05	0.05	0.04	0.04
OCL	–	–	0.01	0.01
Skin	0.01	0.01	0.01	0.01
Kidney (total)	–	–	0.01	0.01
ET region[a]	–	–	0.01	0.01
Remainder tissues	0.05[b]	0.05[b]	–	–
Total	1	1	1	1

[a] ET region: tonsil, larynx, nasal layer, pharynx, tongue.
[b] Remainder tissues: adrenal, brain, pancreas, SI wall, spleen, thymus, muscle, uterus (♀), kidney.

3. Results

3.1. Absorbed dose and effective dose

The absorbed dose to 59 target organs from the 19 investigated radiotracers was calculated in the considered paediatric phantoms. The organ absorbed doses for these radiotracers are provided in supplemental tables A2–A20 (available from stacks.iop.org/PMB/59/1165/mmedia). The highest absorbed dose to critical organs can be observed in the UB wall for ^{11}C-methionine, ^{11}C (realistic maximum model), ^{11}C-4DST and ^{18}F-FBPA; the kidney and UB wall for ^{18}F-L-dopa and ^{68}Ga-EDTA; the pancreas for ^{11}C- and ^{18}F-amino acids; the kidney for ^{11}C-acetate and ^{11}C-thymidine; the liver for [Methyl-^{11}C]-thymidine and ^{11}C-MPDX; the UB wall and GB wall for ^{11}C-brain receptor substances; the liver, spleen, thyroid and testes for ^{15}O-water; the GB wall, stomach wall and thyroid for ^{18}F-brain receptor substances; the heart wall for ^{18}F-FDG; the spleen and thyroid for ^{11}C-SA4503; the GB wall for ^{11}C-TMSX; and the SI wall and stomach wall for ^{11}C-CHIBA-1001, respectively. Figure 2 shows the absorbed doses

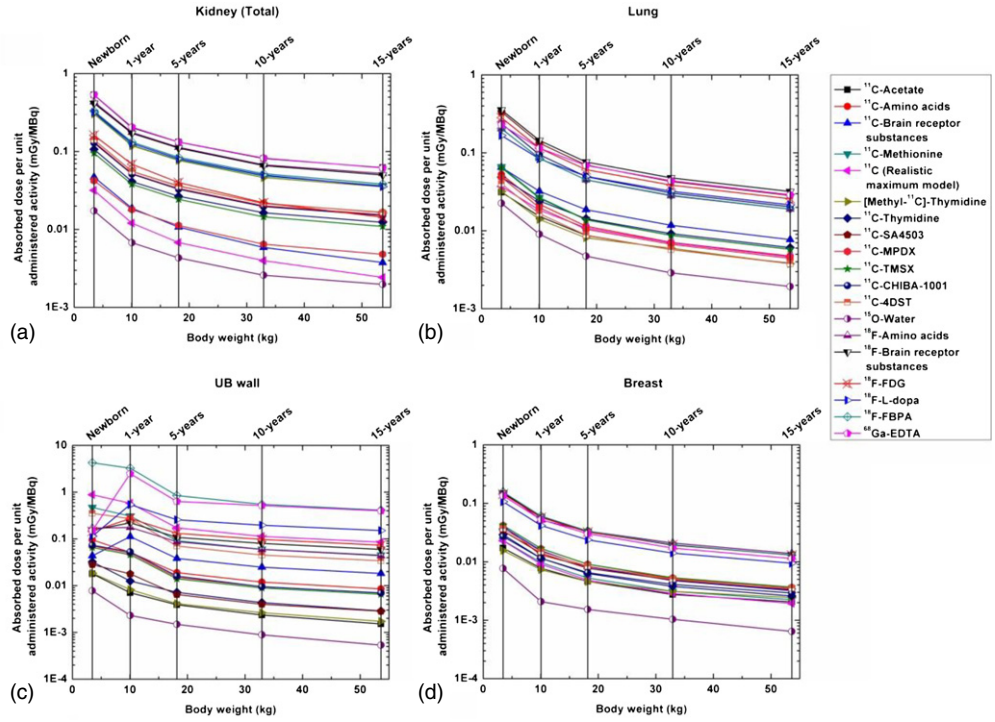

Figure 2. Absorbed dose per unit administered activity (mGy/MBq) of the various PET radiotracers to: (a) the kidney, (b) lung, (c) UB wall and (d) breast of the paediatric female phantoms.

from different radiotracers for the kidney (total), lung, UB wall and breast for the newborn, 1-, 5-, 10- and 15-year-old female models. For most radiotracers, the organ absorbed dose per unit administered activity decreases when the body weight increases. However, for ^{11}C- and ^{18}F-brain receptor substances, ^{18}F-L-DOPA, ^{18}F-FDG, ^{18}F-amino acids and ^{68}Ga-EDTA, the absorbed dose to the UB wall is lower in the newborn than in the 1-year-old child because these radiotracers present with high activity concentration in the UB content and the bladder of the newborn has higher voiding frequency than children at other ages. Among all considered radiotracers, ^{15}O-water produces the lowest absorbed dose to all organs because of the short half-life of the radionuclide (2 min), in contrast to the relatively longer half-lives of F-18 and Ga-68 (110 and 68 min), respectively. Figure 3 shows the absorbed dose per unit administered activity of representative radiotracers to critical organs of the 15-year female model. For organs except kidney, liver and UB wall, the mean absorbed dose of F-18 and Ga-68 labelled radiotracers would be 3.3–5.5 times higher than C-11 labelled radiotracers, and 7.2–21.1 times higher than the absorbed dose from ^{15}O-water.

The effective dose per unit administered activity of 19 radiotracers in the newborn, 1-, 5-, 10- and 15-year-old models calculated using tissue-weighting factors of the ICRP 103 are summarized in table 4. Among the considered radiotracers and paediatric patients at varying ages, ^{18}F-FBPA produces the highest effective dose ranging from 3.37E−02 to 3.43E−01 mSv/MBq while ^{15}O-water produces the lowest effective dose ranging from 1.24E−03 to 1.39E−02 mSv/MBq. ^{68}Ga-EDTA, as an agent for renal function investigation,

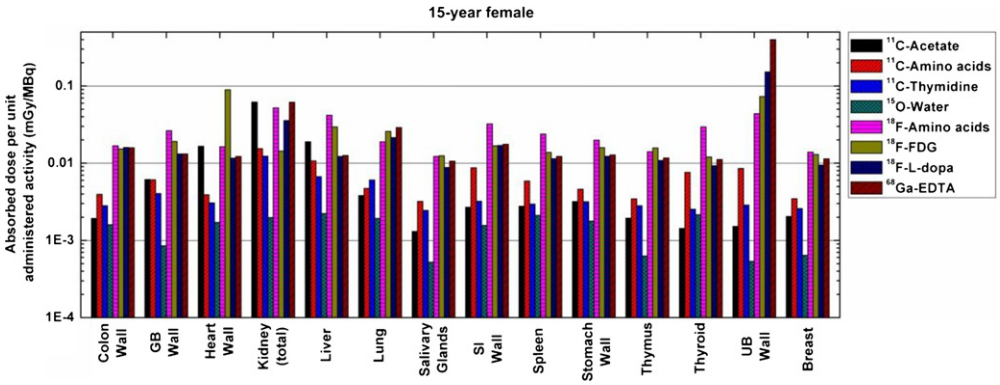

Figure 3. Absorbed dose per unit administered activity (mGy/MBq) to critical organs of the 15-year female for selected radiotracers.

Table 4. Effective dose per unit administered activity of the different radiopharmaceuticals in paediatric phantoms according to the tissue-weighting factors recommended by ICRP Publication 103.

	Effective dose per unit administered activity (mSv/MBq)				
Radiopharmaceutical	Newborn	1 years	5 years	10 years	15 years
^{11}C-Acetate	3.54E-02	1.48E-02	8.75E-03	5.49E-03	3.70E-03
^{11}C-Amino acids	6.09E-02	2.50E-02	1.46E-02	9.52E-03	5.36E-03
^{11}C-Brain receptor substances	4.56E-02	2.34E-02	1.23E-02	7.41E-03	4.84E-03
^{11}C-Methionine	6.20E-02	3.15E-02	1.46E-02	9.26E-03	6.45E-03
[Methyl-^{11}C]-Thymidine	4.06E-02	1.73E-02	1.00E-02	6.79E-03	4.59E-03
^{11}C-Thymidine	3.55E-02	1.45E-02	8.42E-03	5.13E-03	3.30E-03
^{11}C-SA4503	9.61E-02	4.28E-02	2.35E-02	1.37E-02	8.81E-03
^{11}C-MPDX	4.97E-02	2.13E-02	1.16E-02	7.00E-03	4.53E-03
^{11}C-TMSX	5.30E-02	2.24E-02	1.22E-02	7.40E-03	4.79E-03
^{11}C-CHIBA-1001	9.02E-02	3.81E-02	2.15E-02	1.35E-02	8.65E-03
^{11}C-4DST	6.04E-02	2.94E-02	1.35E-02	8.42E-03	5.60E-03
^{15}O-water	1.39E-02	5.89E-03	3.35E-03	2.15E-03	1.24E-03
^{18}F-Amino acids	2.21E-01	9.65E-02	5.81E-02	3.81E-02	2.21E-02
^{18}F-Brain receptor substances	2.98E-01	1.34E-01	7.06E-02	4.32E-02	2.94E-02
^{18}F-FDG	1.76E-01	8.42E-02	4.79E-02	3.03E-02	2.03E-02
^{18}F-L-dopa	1.22E-01	8.00E-02	4.64E-02	3.11E-02	2.19E-02
^{18}F-FBPA	3.43E-01	2.07E-01	7.82E-02	4.87E-02	3.37E-02
^{68}Ga-EDTA	1.59E-01	1.65E-01	6.55E-02	4.56E-02	3.20E-02
^{11}C(Realistic maximum model)	6.69E-02	3.96E-02	1.63E-02	1.05E-02	7.50E-03

delivers a high absorbed dose to the urinary system (kidney and UB) and results in a high effective dose ranging from 3.20E−02 to 1.59E−01 mSv/MBq.

3.2. Dosimetric results from different models

On the basis of the same biokinetic data, we compared the calculated organ absorbed dose and effective dose in the voxel-based paediatric models with the dosimetric estimates published in the ICRP 106 where stylized paediatric phantoms were used. Figure 4 shows the Bland–Altman plots comparing dose estimates to target organs of the 1-, 5- 10- and 15-year-old UF-NCI and

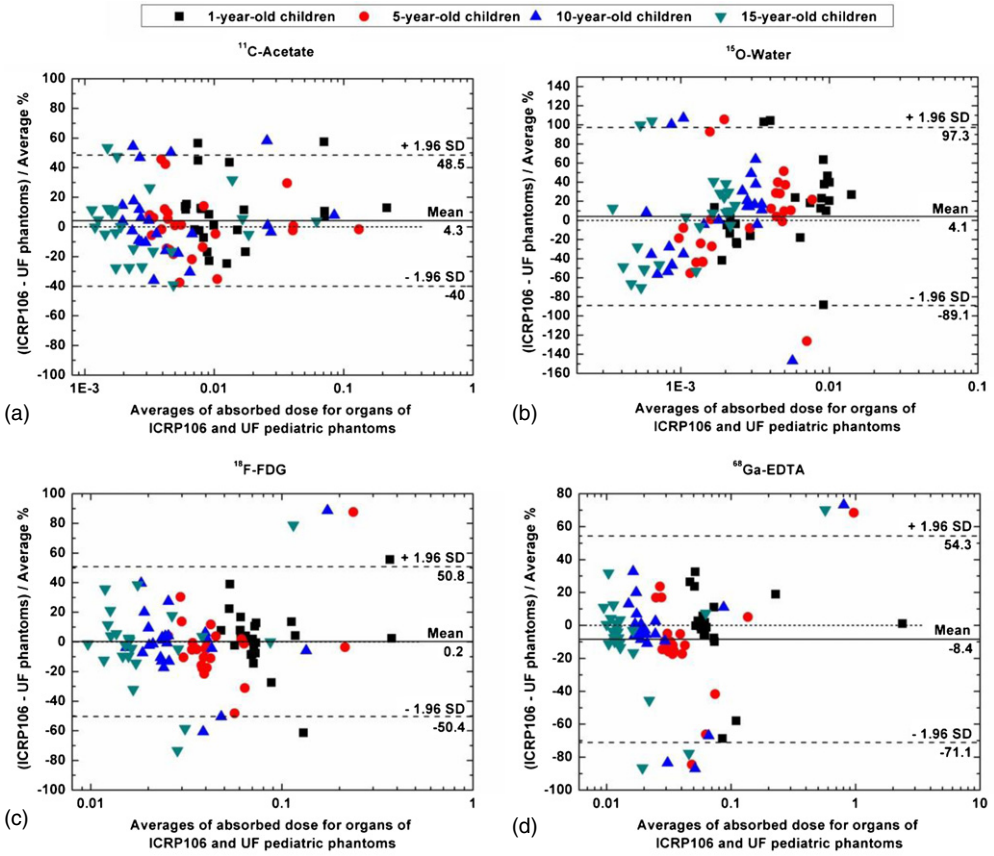

Figure 4. Bland–Altman plots illustrating the percentage difference in sex-averaged absorbed dose of organs ((ICRP106–UF-NCI phantom)/average%) plotted against the mean of sex-averaged absorbed dose ((ICRP106 + UF-NCI phantom)/2) for (a) ^{11}C-acetate, (b) ^{15}O-water, (c)^{18}F-FDG and (d) ^{68}Ga-EDTA of the newborn, 1-year, 5-year, 10-year and 15-year paediatric phantoms.

ICRP paediatric phantoms for representative radiotracers (^{11}C-acetate, ^{15}O-water, ^{18}F-FDG and ^{68}Ga-EDTA). The average percentage differences between organ absorbed doses between the two family of phantoms are 4.3 $\pm$ 22.6% with a 95% confidence interval (CI) of (−40%, 48.5%) for ^{11}C-acetate, 4.1 $\pm$ 47.6% with a 95% CI of (−89.1%, 97.3%) for ^{15}O-water, 0.2 $\pm$ 25.8% with a 95% CI of (−50.4%, 50.8%) for ^{18}F-FDG, and −8.4 $\pm$ 32% with a 95% CI of (−71.1%, 54.3%) for ^{68}Ga-EDTA, respectively. The absorbed dose differences were outside the limits of agreement in six cases (6.3% of all cases) of spleen, pancreas and cortical bone for ^{11}C-acetate, nine cases (9.4% of all cases) of testes, cortical bone and bone marrow for ^{15}O-water, in nine cases (9.4% of all cases) of uterus, ovaries and bladder for ^{18}F-FDG, and in ten cases (10.4% of all cases) of uterus, ovaries, lung and bladder for ^{68}Ga-EDTA. Organ absorbed dose differences were equally distributed and unbiased across the mean dose range for ^{11}C-acetate and ^{18}F-FDG, while the percentage difference presented a positive correlation to the magnitude of organ absorbed dose for ^{15}O-water. Organs absorbed dose of ICRP 106 at 64.5% of the data points for ^{68}Ga-EDTA is lower than those of the UF-NCI phantoms.

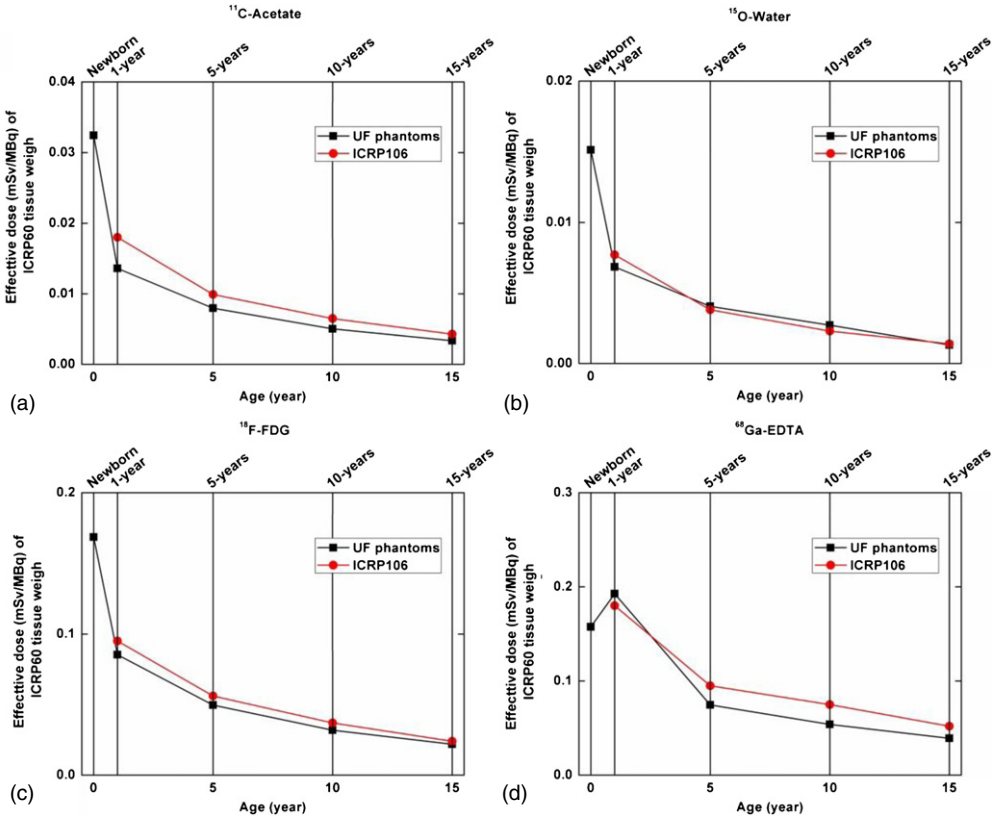

Figure 5. Comparison of the effective dose between this work (UF-NCI phantoms) and the ICRP106 for: (a) ^{11}C-acetate, (b) ^{15}O-water, (c)^{18}F-FDG and (d) ^{68}Ga-EDTA of the newborn, 1-year, 5-year, 10-year and 15-year paediatric phantoms.

Figure 5 shows the calculated effective dose to the UF-NCI phantoms using ICRP 60 weighting factors and kinetic data provided in the ICRP 106 for representative radiotracers. The effective dose of ICRP 106 for most paediatric models at different ages is slightly higher than that of UF-NCI phantoms. The relative differences of the effective dose between stylized and voxel-based phantoms are $-22.2 \pm 1.9\%$, $1.8 \pm 13.3\%$, $-11.0 \pm 2.3\%$, and $-16.8 \pm 16.1\%$ for ^{11}C-Acetate, ^{15}O-Water, ^{18}F-FDG and ^{68}Ga-EDTA, respectively.

3.3. Influence of ICRP103 dosimetry schema on effective dose calculation

Figure 6 compares effective doses in the UF-NCI paediatric phantoms for the 19 considered positron-emitting labelled radiotracers using the same biokinetic data and tissue-weighting factors of the ICRP 60 and ICRP 103, respectively. As shown in figure 6(a), for ^{11}C-Acetate, the new ω_T of the ICRP 103 increases the effective dose to the paediatric models by 9.6%. For ^{11}C-thymidine, ^{11}C-SA4503, ^{11}C-MPDX, ^{11}C-TMSX and ^{11}C-CHIBA-1001, the effective doses calculated using weighting factors of the ICRP 103 are about 2.5% lower than those calculated using the ICRP 60 factors at all ages. For other radiotracers, the ratios of the effective doses obtained using ICRP 60 to ICRP 103 vary between 0.96 and 1.36, where the new ω_T of ICRP 103 generate lower effective doses than the old ω_T of the ICRP 60 in

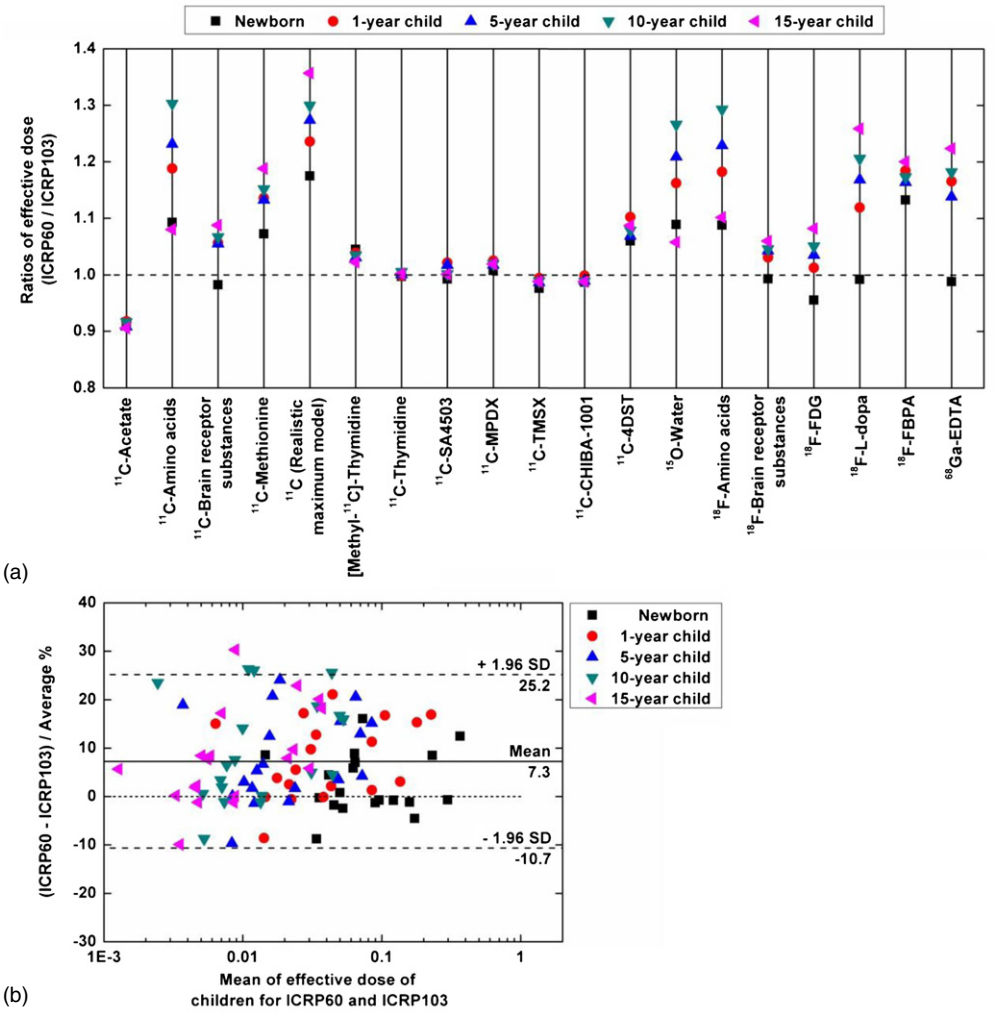

Figure 6. (a) Ratios of effective doses calculated using tissue-weighting factors of ICRP60 and ICRP103 when using the evaluated radiotracers for the newborn, 1-year, 5-year, 10-year and 15-year paediatric models. (b) Bland–Altman plot illustrating the percentage difference in effective doses ((ICRP60–ICRP103)/average%) plotted against the mean effective doses ((ICRP60 + ICRP103)/2) for various radiotracers of paediatric phantoms.

all paediatric phantoms, except for the newborn. The Bland–Altman analysis (figure 6(b)) demonstrates a good agreement between the effective doses for 19 radiotracers when using the weighting factors recommended in both ICRP reports. The mean relative difference between effective doses from ICRP 60 to ICRP 103 tissue-weighting factors is 7.3 ± 9.1% with a 95% CI of (−10.7%, 25.2%). The mean relative difference of effective doses between the two recommended tissue-weighting factors for all studied radiotracers are 2.9 ± 6.6%, 8.3 ± 8.8%, 8.9 ± 10.2%, 10.9 ± 12.1% and 9.0 ± 11.1% for the newborn, 1-, 5- 10- and 15-year-old paediatric models, respectively.

Table 5. Paediatric dose regimens and associated formulas for ^{18}F-FDG.

Rule	Formula
North American consensus, max level[a]	5.2 × Body mass(kg), min = 37 MBq
North American consensus, min level[a]	3.7 × Body mass(kg)
EANM dose card	(Lassmann *et al* 2007)
NECRD method[b]	14.8 × exp[0.046 × body mass(kg)]
Weight category-based dose card	(Alessio *et al* 2009)
Clark's formula[c]	(Body mass (kg) × adult dose)/70
BSA-based formula[d]	(BSA(m^2) × adult dose)/1.73
Webster's formula[e]	(Age(y) + 7) × (adult dose)/(Age(y) + 1)

[a] Gelfand *et al* (2011).
[b] Accorsi *et al* (2010).
[c] Accorsi *et al* (2010), Churchill (1964).
[d] The BSA is calculated using the body surface area formula of Du Bois *et al* (Gelfand 2010, Gelfand *et al* 2011, Du Bois and Du Bois 1916, 1989).
[e] Gelfand *et al* (2011), Accorsi *et al* (2010).

3.4. ^{18}F-FDG radiation dose from different regimens

Seven ^{18}F-FDG-PET dose regimens used in different facilities and reported in recent publications (table 5) were used to estimate the injected activity of ^{18}F-FDG for the reference paediatric patients of different ages where the reference activity for adults is assumed to be 370 MBq according to protocols used in our institution. Figure 7(a) presents the recommended administered activity of ^{18}F-FDG for children when using different dosing strategies whereas figure 7(b) compares the resulting effective doses to the female models. In ^{18}F-FDG imaging, the effective dose for paediatric patients may vary from 1.7 to 9.4 mSv when using the different dose regimens. For 1-, 5- and 10-year-old reference paediatric models, the lowest effective dose is produced by the dose regimen suggested by Accorsi *et al* (2010) (2.0, 1.7 and 2.1 mSv, respectively). For the newborn, the minimum level of the North American consensus guideline and EANM dose card generate the lowest and second lowest effective dose (2.3 and 2.5 mSv, respectively) whereas the EANM dose card produces the lowest effective dose to the 15-year-old model (3.4 mSv). In the ^{18}F-FDG PET scans, the source organs containing high activity concentration include UB content, heart wall, brain, liver and the lungs. Figure 8 shows the absorbed dose to the heart wall and UB wall for ^{18}F-FDG when using different dosing strategies. Similar to the effective dose, the absorbed dose to the heart wall and UB wall of the different paediatric phantoms vary from 7.4 to 48.5 mGy and from 1.9 to 24.7 mGy, respectively for the various dose regimens.

3.5. Effect of human/mouse-derived biokinetic data on paediatric dosimetry

Figure 9 compares human/mouse-derived organ absorbed dose and effective dose for the paediatric models at different ages for some radiotracers (^{11}C-SA4503, ^{11}C-MPDX, ^{11}C-TMSX, ^{11}C-CHIBA-1001, ^{11}C-4DST and ^{18}F-FBPA). Figure 9(a) shows the Bland–Altman plots comparing human/mouse-derived organ absorbed doses for the different anatomical models. The mean relative difference between organ absorbed doses resulting from the use of human- to mouse-derived calculations is 5.5 ± 44.4% with a 95% CI of (−81.7%, 92.6%). The absolute difference for 18.1% of the data points is higher than 50%. The ratios between human- and mouse-derived effective doses for the paediatric phantoms are shown in figure 9(b). The mean ratios for ^{11}C-SA4503, ^{11}C-MPDX, ^{11}C-TMSX, ^{11}C-CHIBA-1001, ^{11}C-4DST and

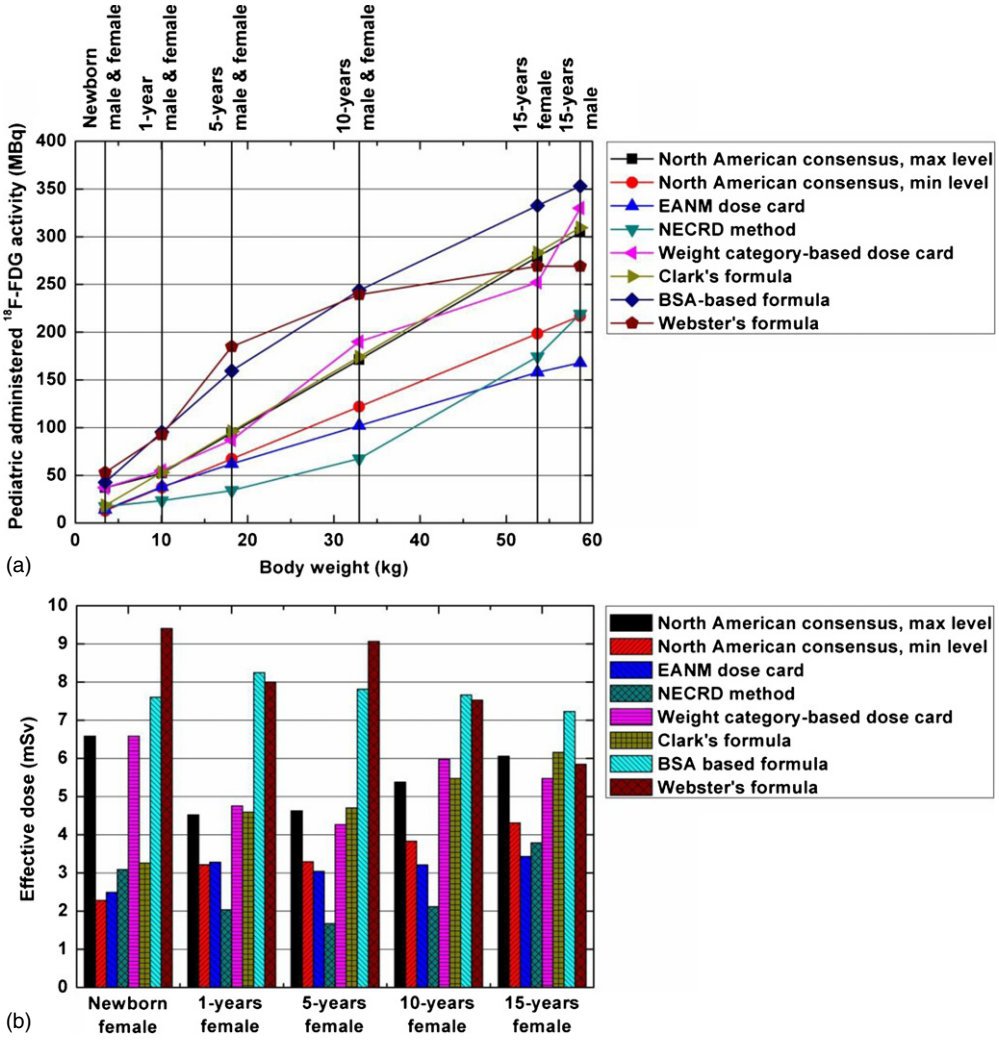

Figure 7. (a) Recommended injected activity of ^{18}F-FDG for paediatric patients at different ages when using the various dose regimens. (b) The effective dose (mSv) to the paediatric female phantoms of ^{18}F-FDG from the recommended injected activities at various dose regimens.

^{18}F-FBPA are 1.9, 1.0, 1.2, 1.6, 0.8 and 1.3, respectively. This is in agreement with results reported by Sakata *et al* (2013) for adults.

4. Discussion

The development of novel molecular PET imaging probes produced by labelling biological molecules with positron-emitting radionuclides is an active research field (Valliant 2010). Accurate dosimetry calculations for representative groups of paediatric patients is needed to optimize the dose regimens of various radiotracers and to investigate the collective radiation exposure and risks associated with nuclear medicine procedures. In this work, we estimated

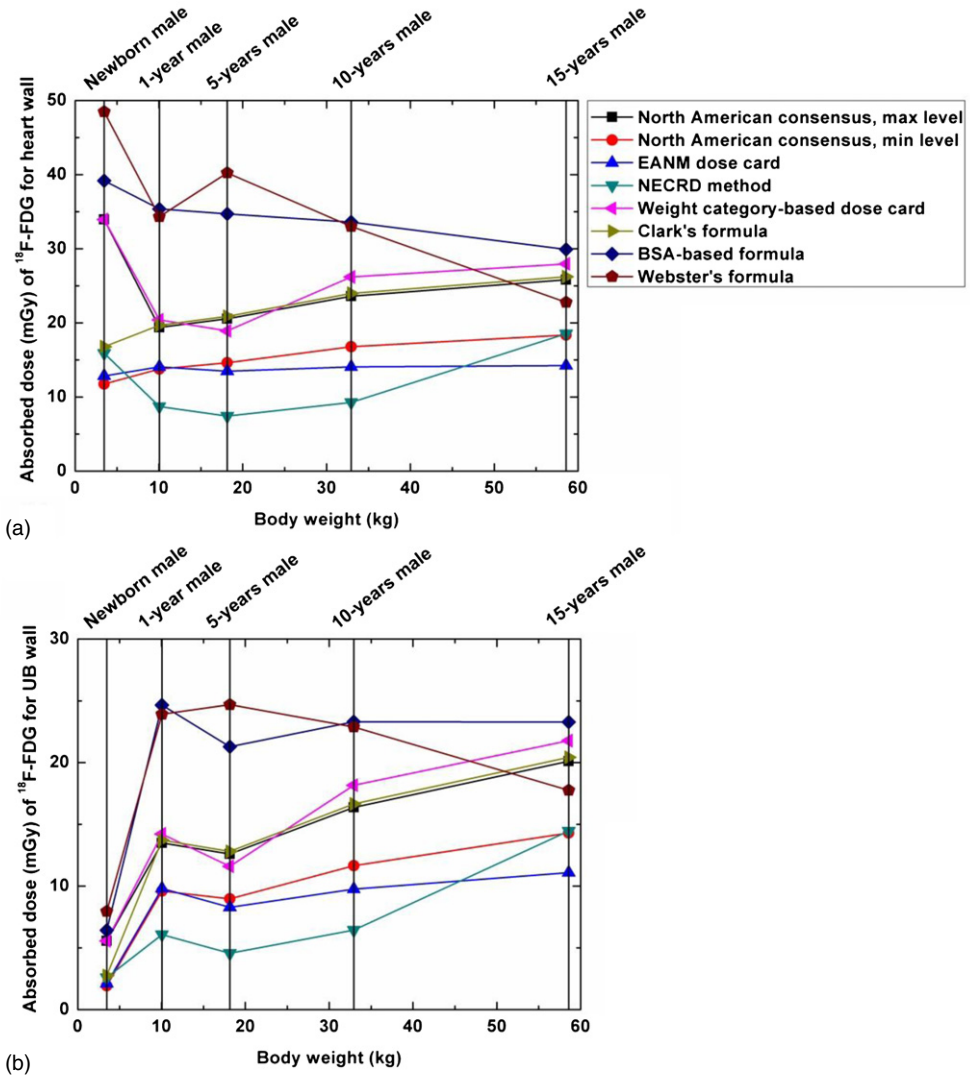

Figure 8. Absorbed dose (mGy) of ^{18}F-FDG in (a) the heart wall and (b) UB wall of the paediatric male phantoms when using the various dose regimens.

organ absorbed dose and effective dose using new generation of reference age and sex-dependent computational paediatric phantoms and the latest dosimetric data available for 19 positron-emitting labelled radiotracers. For the evaluated radiotracers, the organ absorbed dose may vary from 2.68×10^{-4} to 12.9 mGy/MBq depending on the physical half-life of the radionuclide and the biological half-life and biodistribution of the radiotracer. In general, F-18 and Ga-68 labelled radiotracers produce a higher absorbed dose in most organs and result in higher effective dose for paediatric patients compared to C-11 and O-15 labelled radiotracers, because of the longer physical half-life.

We studied the effect of the type of anthropomorphic model, dosimetric and biokinetic data and dose regimens on internal radiation dose calculations from various radiotracers to the

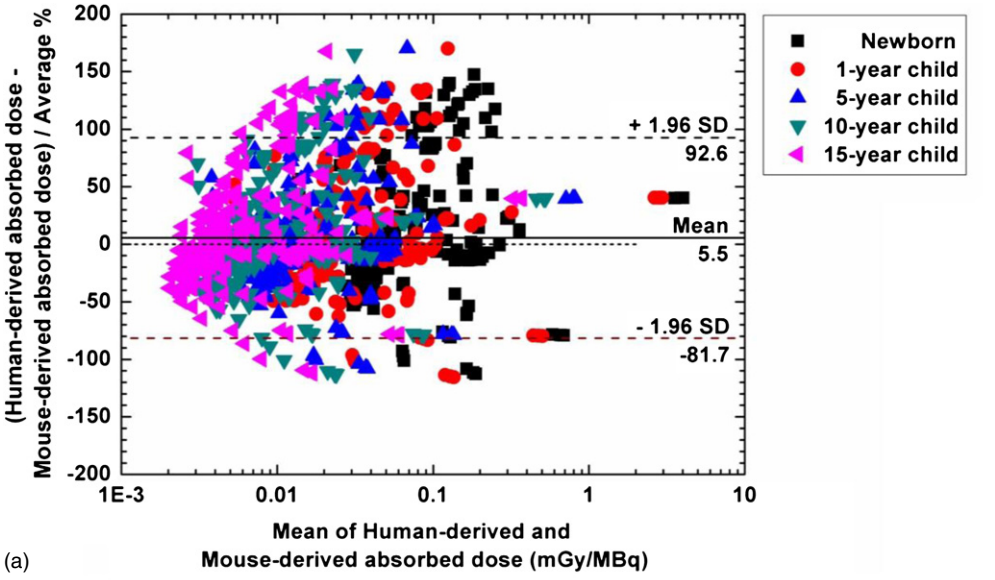

(a)

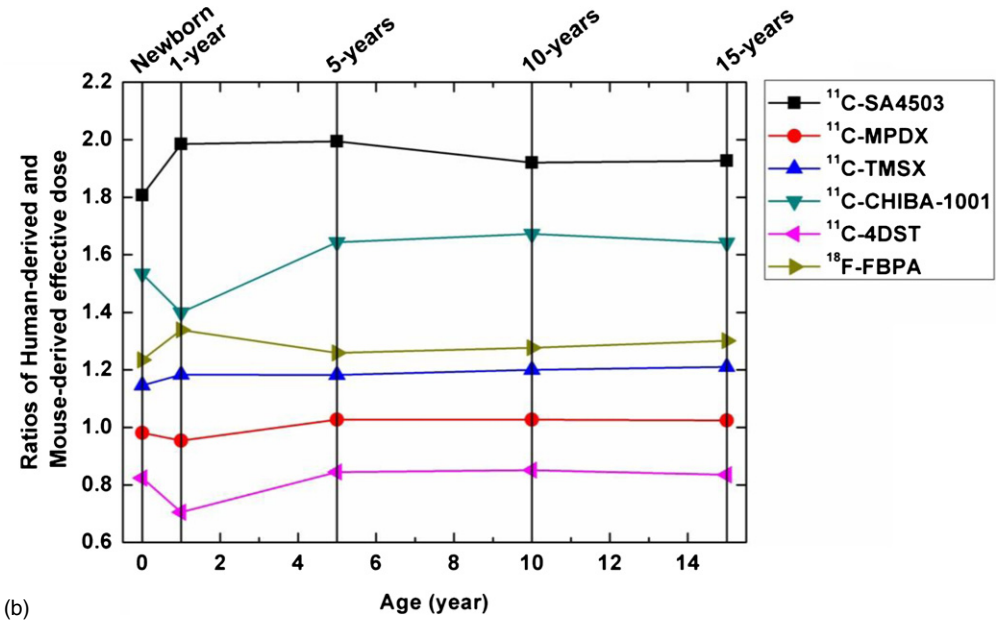

(b)

Figure 9. (a) Bland–Altman plots illustrating the percentage difference between human- and mouse-derived absorbed doses of organs plotted against the mean absorbed doses for different radiotracers. (b) Ratios of human-derived to mouse-derived effective doses for different radiotracers of paediatric phantoms.

paediatric population. A large difference is observed for some organ absorbed dose between the MIRD-type and the voxel-based phantoms. The absolute difference for about 34% of organs is higher than 20%, especially, for spleen, pancreas, uterus, cortical bone, bone marrow, gonads, lung and bladder. The absorbed dose difference is out of the 95% CI for some radiotracers

and some organs. The MIRD-type phantom overestimates the effective dose by 6.8%–39% compared to its voxel-based model counterpart in most paediatric phantoms for the selected radiotracers. The ICRP publication 103 (ICRP 2007) proposed new tissue-weighting factors for the calculation of the effective dose for radiation protection purposes where the breast weighting factor increased from 0.05 to 0.12. For anterior–posterior geometry in external radiation exposure, the new ICRP 103 ω_T produces moderate impact on the effective dose for photon energies below 0.1 MeV and electron energies between 1 and 4 MeV (ICRP 2010). The effect is definitely energy- and geometry-dependent and there are energies and geometries for which effective doses according to ICRP 103 are higher than those of ICRP 60 and vice versa (Boetticher *et al* 2008). However, in internal radiation dosimetry, the breast is not the critical organ and as such, the change of the breast weighting factor plays a minor role in the calculation of the effective dose for PET radiotracers. As shown in table 3, the gonads (ovaries and testes) weighting factors decreased significantly from 0.2 in ICRP 60 to 0.08 in ICRP 103. Accordingly, the effective dose reduced the overall contribution of the gonads dose to the total dose. The gonads dose depends on the cumulated activity of radiotracers in the ovaries/testes for self-irradiation and in adjacent organs, such as the UB, for cross-irradiation. The increased tissue-weighting factors for critical organs, such as the heart wall and kidneys explains the increase of the effective dose. For ^{11}C-acetate, the gonads and UB have low activity concentration whereas the heart wall and kidney have significantly high activity than other organs. The effective dose calculated using ICRP 103 weighting factors is about 10% higher than the one obtained using ICRP 60. For radiotracers such as ^{18}F-FBPA, the highest cumulated activity is present in the UB of all organs. The effective dose using the new ω_T decreased by about 14%. In this work, the bladder of the newborn was assumed to have high voiding frequency, which results in a low cumulated activity for the UB and low cross-absorbed dose to the gonads of the newborn. Therefore, the newborn's effective dose for most radiotracers is less influenced by changes in ω_T compared to other paediatric models.

A variety of dose regimens were proposed to determine the optimal injected activity for paediatric patients. Popular dose regimens can be roughly classified into five classes: weight-based rules, such as Clark's formula (Accorsi *et al* 2010, Churchill 1964), the North American consensus guideline (Gelfand *et al* 2011); body surface area-based rule (Gelfand 2010, Gelfand *et al* 2011, Du Bois and Du Bois 1916, 1989); age-based rule (Gelfand *et al* 2011, Accorsi *et al* 2010); the dose cards of the EANM (Lassmann *et al* 2007) and weight category-based dose card proposed by Alessio *et al* (2009); and the patient-specific noise-equivalent count rate density method developed by Accorsi *et al* (2010). In the North American consensus guideline for ^{18}F-FDG, the low end of the dose range should be considered for smaller patients, and the administered activity may take into account patient's weight and time available on the PET scanner. Different dose regimens would result in significantly different levels of injected activity and thus effective dose for the paediatric population. In the case of ^{18}F-FDG and the newborn as model, Webster's formula produces the highest effective dose, which is about three times higher than the effective dose produced by the EANM dose card. Overall, the minimum level of the North American consensus guideline generates the lowest effective dose in the newborn. The dose regimen proposed by Accorsi *et al* produced the lowest effective dose for 1-, 5- and 10-year-old models, whereas the EANM dose card produced the lowest and secondary lowest effective dose for 15-year-old and the newborn models, respectively. In this context, the dose regimen of Accorsi *et al* and the EANM dose card produce the lowest effective doses compared to other dose regimens for the reference paediatric models.

The use of human- versus and mouse-derived biokinetic data result in noticeable discrepancy between organ absorbed dose and effective dose estimates for the paediatric population. The absorbed dose and effective dose differences vary from −115.6% to 170.2%

and from −29.5% to 99.5%, respectively. Similar to observations made for adults, the use of mouse-derived biokinetic data is often not satisfactory enough for assessing the absorbed dose distributions and radiation risks in paediatric radiation dosimetry. Consequently, biodistribution and biokinetic studies in humans are required for most novel molecular imaging probes.

5. Conclusion

A methodical study was conducted to evaluate the radiation dose from positron-emitting labelled radiotracers to the paediatric population using the latest generation anthropomorphic computational phantoms and updated tissue-weighting factors. We also investigated the impact of different types of anthropomorphic models, tissue-weighting factors, dose regimens and biokinetic data on the resulting organ absorbed dose and effective dose. Model-specific differences of the effective dose were observed on paediatric phantoms at different age for most radiotracers. For most radiotracers with low activity concentration in the breast, the implementation of ICRP 103 tissue-weighting factors decreases the estimated effective dose to paediatric patients. The various dose regimens provide different levels of injected activity and as such result in high effective dose to some cases. The choice of a suitable dose regimen in clinical practice will significantly reduce the radiation risks for paediatric patients. The calculation of the effective dose strongly depends on the biodistribution and biokinetic data of radiotracers. Consequently, human-based biokinetic studies are often desired for most new PET imaging probes. The generated database of organ absorbed dose and effective dose for various positron-emitting labelled radiotracers can be used to assess the radiation risks to the paediatric population in clinical PET imaging procedures.

Acknowledgments

This work was supported by Geneva Cancer League and Geneva University Hospital under grant PRD 11-II-1. The authors would like to thank Dr WE Bolch (University of Florida) and Dr C Lee (National Cancer Institute/NIH) for providing the paediatric models.

Appendix

The radiation absorbed dose $D\,(r_T, T_D)$ delivered to any target tissue r_T from source organ r_S, over a considered dose-integration period T_D is given by:

$$D\,(r_T, T_D) = \sum_{r_S} \int_0^{T_D} A(r_S, t) S(r_T \leftarrow r_S)\,\mathrm{d}t = \sum_{r_S} \tilde{A}(r_S, T_D) S(r_T \leftarrow r_S) \tag{A.1}$$

where $A(r_S, t)$ and $\tilde{A}(r_S, T_D)$ are the time-dependent activity and the cumulated (time-integrated) activity of the radiotracer in the source region, respectively. $S(r_T \leftarrow r_S)$ is the S-value describing the equivalent dose rate in the target organ per unit activity in the source organ.

The equivalent dose $H\,(r_T, T_D)$ is given by:

$$H\,(r_T, T_D) = \sum_R \omega_R D_R\,(r_T, T_D) \tag{A.2}$$

where the ω_R is the radiation weighting factor for radiation type R, and $D_R\,(r_T, T_D)$ is the contribution of radiation type R to the absorbed dose. In diagnostic nuclear medicine, the ICRP-recommended values of ω_R are 1.0 for photons, electrons and positrons.

The effective dose E is given by

$$E = \sum_T \omega_T H\left(r_T, T_D\right) \tag{A.3}$$

where ω_T is the tissue-weighting factor for organ/tissue T reflecting its relative radiation sensitivity.

The absorbed dose to the target tissue per unit administered activity is given by

$$d\left(r_T, T_D\right) = \frac{D\left(r_T, T_D\right)}{A_0} = \sum_{r_S} \frac{\tilde{A}\left(r_S, T_D\right)}{A_0} S\left(r_T \leftarrow r_S\right). \tag{A.4}$$

The effective dose in the human body per unit administered activity is given by

$$\tilde{E} = \frac{E}{A_0} = \sum_T \omega_T \sum_R \omega_R \frac{D_R\left(r_T, T_D\right)}{A_0} = \sum_T \omega_T \sum_R \omega_R d_R\left(r_T, T_D\right). \tag{A.5}$$

The effective dose is given by

$$E = \sum_T \omega_T \left[\frac{H^{\text{Male}}_{\left(r_T, D_T\right)} + H^{\text{Female}}_{\left(r_T, D_T\right)}}{2}\right]. \tag{A.6}$$

References

Accorsi R, Karp J S and Surti S 2010 Improved dose regimen in pediatric PET *J. Nucl. Med.* **51** 293–300

Albrecht S, Buchegger F, Soloviev D, Zaidi H, Vees H, Khan H G, Keller A, Delaloye A B, Ratib O and Miralbell R 2007 11C-acetate PET in the early evaluation of prostate cancer recurrence *Eur. J. Nucl. Med. Mol. Imaging* **34** 185–96

Alessio A M, Kinahan P E, Manchanda V, Ghioni V, Aldape L and Parisi M T 2009 Weight-based, low-dose pediatric whole-body PET/CT protocols *J. Nucl. Med.* **50** 1570–8

Alessio A M, Sammer M, Phillips G S, Manchanda V, Mohr B C and Parisi M T 2011 Evaluation of optimal acquisition duration or injected activity for pediatric 18F-FDG PET/CT *J. Nucl. Med.* **52** 1028–34

Boetticher H, Lachmund J, Looe H K, Hoffmann W and Poppe B 2008 2007 recommendations of the ICRP change basis for estimation of the effective dose: what is the impact on radiation dose assessment of patient and personnel? *Rofo* **180** 391–5

Bolch W E, Eckerman K F, Sgouros G and Thomas S R 2009 MIRD pamphlet no. 21: a generalized schema for radiopharmaceutical dosimetry—standardization of nomenclature *J. Nucl. Med.* **50** 477–84

Chawla S C, Federman N, Zhang D, Nagata K, Nuthakki S, McNitt-Gray M and Boechat M I 2010 Estimated cumulative radiation dose from PET/CT in children with malignancies: a 5-year retrospective review *Pediatr. Radiol.* **40** 681–6

Churchill J A 1964 Posology in infants and children *Dev. Med. Child Neurol.* **6** 610–3

Du Bois D and Du Bois E F 1916 Clinical calorimetry: tenth paper a formula to estimate the approximate surface area if height and weight be known *Arch. Intern. Med.* **17** 863–71

Du Bois D and Du Bois E F 1989 A formula to estimate the approximate surface area if height and weight be known *Nutrition* **5** 303–11 (PMID: 2520314)

Eberlein U, Bröer J H, Vandevoorde C, Santos P, Bardiès M, Bacher K, Nosske D and Lassmann M 2011 Biokinetics and dosimetry of commonly used radiopharmaceuticals in diagnostic nuclear medicine—a review *Eur. J. Nucl. Med. Mol. Imaging* **38** 2269–81

Fahey F H, Treves S T and Adelstein S J 2011 Minimizing and communicating radiation risk in pediatric nuclear medicine *J. Nucl. Med.* **52** 1240–51 (PMID: 21764783)

Gambhir S S 2002 Molecular imaging of cancer with positron emission tomography *Nature Rev. Cancer* **2** 683–93

Gelfand M 2010 Dose reduction in pediatric hybrid and planar imaging *Q. J. Nucl. Med. Mol. Imaging* **54** 379–88 (PMID: 20823806)

Gelfand M J, Parisi M T and Treves S T 2011 Pediatric radiopharmaceutical administered doses: 2010 North American consensus guidelines *J. Nucl. Med.* **52** 318–22

Goethals P, Lameire N, van Eijkeren M, Kesteloot D, Thierens H and Dams R 1996 [Methyl-carbon-11] thymidine for *in vivo* measurement of cell proliferation *J. Nucl. Med.* **37** 1048–52

HPS 2013 http://hps.org/publicinformation/radardecaydata.cfm

Huang C and McConathy J 2013 Radiolabeled amino acids for oncologic imaging *J. Nucl. Med.* **54** 1–4

ICRP 1988 Radiation dose to patients from radiopharmaceuticals *ICRP Publication* 53 *Ann. ICRP* **18** 1–76

ICRP 1991 1990 recommendations of the International Commission on Radiological Protection *ICRP Publication* 60 *Ann. ICRP* **21** 1–77

ICRP 1998 Radiation dose to patients from radiopharmaceuticals (addendum 2 to ICRP publication 53) *Ann. ICRP* **28** 1–126

ICRP 2007 The 2007 recommendations of the International Commission on Radiological Protection *ICRP Publication* 103 *Ann. ICRP* **37** 1–332

ICRP 2008 Radiation dose to patients from radiopharmaceuticals—addendum 3 to ICRP Publication 53 *ICRP Publication* 106 *Ann. ICRP* **38** 1–197

ICRP 2010 Conversion coefficients for radiological protection quantities for external radiation exposures *ICRP Publication* 116 *Ann. ICRP* **40** 1–257

Jacobs F, Thierens H, Piepsz A, Bacher K, Van De Wiele C, Ham H and Dierckx R 2005 Optimised tracer-dependent dosage cards to obtain weight-independent effective doses *Eur. J. Nucl. Med. Mol. Imaging* **32** 581–8

Kleis M, Daldrup-Link H, Matthay K, Goldsby R, Lu Y, Schuster T, Schreck C, Chu P W, Hawkins R A and Franc B L 2009 Diagnostic value of PET/CT for the staging and restaging of pediatric tumors *Eur. J. Nucl. Med. Mol. Imaging* **36** 23–36

Lassmann M, Biassoni L, Monsieurs M, Franzius C and Jacobs F 2007 The new EANM paediatric dosage card *Eur. J. Nucl. Med. Mol. Imaging* **34** 796–8

Maecke H and André J 2007 *PET Chemistry* (New York: Springer) pp 215–42

Mishina M, Ishiwata K, Naganawa M, Kimura Y, Kitamura S, Suzuki M, Hashimoto M, Ishibashi K, Oda K and Sakata M 2011 Adenosine A2A receptors measured with [11C] TMSX PET in the striata of Parkinson's disease patients *PLoS One* **6** e17338

Mothersill C and Seymour C 2014 Implications for human and environmental health of low doses of ionising radiation *J. Environ. Radioact.* at press (PMID: 23664231)

Nesterov S V, Han C, Mäki M, Kajander S, Naum A G, Helenius H, Lisinen I, Ukkonen H, Pietilä M and Joutsiniemi E 2009 Myocardial perfusion quantitation with 15O-labelled water PET: high reproducibility of the new cardiac analysis software (Carimas™) *Eur. J. Nucl. Med. Mol. Imaging* **36** 1594–602

Oehme L, Perick M, Beuthien-Baumann B, Wolz M, Storch A, Löhle M, Herting B, Langner J, van den Hoff J and Reichmann H 2011 Comparison of dopamine turnover, dopamine influx constant and activity ratio of striatum and occipital brain with 18F-dopa brain PET in normal controls and patients with Parkinson's disease *Eur. J. Nucl. Med. Mol. Imaging* **38** 1550–9

Parker M S, Hui F K, Camacho M A, Chung J K, Broga D W and Sethi N N 2005 Female breast radiation exposure during CT pulmonary angiography *Am. J. Roentgenol* **185** 1228–33

Paul S, Elsinga P H, Ishiwata K, Dierckx R A and van Waarde A 2011 Adenosine A1 receptors in the central nervous system: their functions in health and disease, and possible elucidation by PET imaging *Curr. Med. Chem.* **18** 4820–35

Petoussi-Henss N, Zankl M, Hoeschen C and Nosske D 2007 Voxel or MIRD-type model: a sensitivity study relevant to nuclear medicine *World Congress on Medical Physics and Biomedical Engineering 2006* (Berlin: Springer) pp 2061–4

Prasad K N, Cole W C and Hasse G M 2004 Health risks of low dose ionizing radiation in humans: a review *Exp. Biol. Med.* **229** 378–82 (PMID: 15096649)

Reivich M *et al* 1985 Glucose metabolic rate kinetic model parameter determination in humans: the lumped constant and rate constants for [^{18}F]fluorodeoxyglucose and [^{11}C]deoxyglucose *J. Cereb. Blood Flow Metab.* **5** 179–92

Robbins E 2008 Radiation risks from imaging studies in children with cancer *Pediatr. Blood Cancer* **51** 453–7

Sakata M, Oda K, Toyohara J, Ishii K, Nariai T and Ishiwata K 2013 Direct comparison of radiation dosimetry of six PET tracers using human whole-body imaging and murine biodistribution studies *Ann. Nucl. Med.* **27** 285–96

Sillen U 2001 Bladder function in healthy neonates and its development during infancy *J. Urol.* **166** 2376–81

Stabin M G 1996 MIRDOSE: personal computer software for internal dose assessment in nuclear medicine *J. Nucl. Med.* **37** 538–46 (PMID: 8772664)

Stabin M G, Sparks R B and Crowe E 2005 OLINDA/EXM: the second-generation personal computer software for internal dose assessment in nuclear medicine *J. Nucl. Med.* **46** 1023–7 (PMID: 15937315)

Steinert M, Weiss M, Gottlöber P, Belyi D, Gergel O, Bebeshko V, Nadejina N, Galstian I, Wagemaker G and Fliedner T M 2003 Delayed effects of accidental cutaneous radiation exposure: fifteen years of follow-up after the Chernobyl accident *J. Am. Acad. Dermatol.* **49** 417–23

Tatsumi M, Miller J H and Wahl R L 2007 18F-FDG PET/CT in evaluating non-CNS pediatric malignancies *J. Nucl. Med.* **48** 1923–31

Toyohara J, Nariai T, Sakata M, Oda K, Ishii K, Kawabe T, Irie T, Saga T, Kubota K and Ishiwata K 2011 Whole-body distribution and brain tumor imaging with 11C-4DST: a pilot study *J. Nucl. Med.* **52** 1322–8

Toyohara J, Sakata M and Ishiwata K 2009 Imaging of sigma1 receptors in the human brain using PET and [11C] SA4503 *Cent. Nerv. Syst. Agents Med. Chem.* **9** 190–6

Treves S T, Baker A, Fahey F H, Cao X, Davis R T, Drubach L A, Grant F D and Zukotynski K 2011 Nuclear medicine in the first year of life *J. Nucl. Med.* **52** 905–25

Treves S T, Davis R T and Fahey F H 2008 Administered radiopharmaceutical doses in children: a survey of 13 pediatric hospitals in North America *J. Nucl. Med.* **49** 1024–7

Valliant J F 2010 A bridge not too far: linking disciplines through molecular imaging probes *J. Nucl. Med.* **51** 1258–68

Visser F C 2001 Imaging of cardiac metabolism using radiolabelled glucose, fatty acids and acetate *Coron. Artery Dis.* **12** S12–18 (PMID: 11286301)

Xie T, Bolch W E, Lee C and Zaidi H 2013 Pediatric radiation dosimetry for positron-emitting radionuclides using anthropomorphic phantoms *Med. Phys.* **40** 102502

Yoshimoto M, Kurihara H, Honda N, Kawai K, Ohe K, Fujii H, Itami J and Arai Y 2013 Predominant contribution of L-type amino acid transporter to 4-borono-2–^{18}F-fluoro-phenylalanine uptake in human glioblastoma cells *Nucl. Med. Biol.* **40** 625–9

Zaidi H 1999 Relevance of accurate Monte Carlo modeling in nuclear medical imaging *Med. Phys.* **26** 574–608

Zaidi H and Xu G 2007 Computational anthropomorphic models of the human anatomy: the path to realistic Monte Carlo modeling in radiological sciences *Annu. Rev. Biomed. Eng.* **9** 471–500